because the exact dependence of the free volume as a function of temperature and composition is not known. However, there does seem to be a change in slope, and hence β', in the range of the boiling point of chloroform.

Acknowledgment. The financial support of the donors of the Petroleum Research Fund, administered by the American Chemical Society, the Research Corp., the Drexel University Graduate School, and the Drexel University Computer Center is gratefully acknowledged. We also wish to thank the reviewers for helpful suggestions.

References and Notes

(1) Bailey, R. T.; North, A. M.; Pethrick, R. A. "Molecular Motion in High Polymers"; Clarendon Press: Oxford, 1981.
(2) Heatley, F. *Prog. NMR Spectrosc.* **1979**, *13*, 47.
(3) Schaefer, J. *Macromolecules* **1973**, *6*, 882.
(4) Valeur, B.; Jarry, J. P.; Geny, F.; Monnerie, L. *J. Polym. Sci., Polym. Phys. Ed.* **1975**, *13*, 667, 675, 2251.
(5) Bendler, J. T.; Yaris, R. *Macromolecules* **1978**, *11*, 650.
(6) Skolnick, J.; Yaris, R. *Macromolecules* **1982**, *15*, 1041.
(7) Skolnick, J.; Yaris, R. *Macromolecules* **1982**, *15*, 1046.
(8) Skolnick, J.; Yaris, R. *Macromolecules* **1983**, *16*, 266.
(9) For correction to ref 6, see: Yamakawa, H. *Macromolecules* **1983**, *16*, 491.
(10) Leitch, L. C. *Can. J. Chem.* **1957**, *35*, 345.
(11) Cockburn, W. F.; Hubley, C. E. *Appl. Spectrosc.* **1957**, *4*, 188.
(12) Brandrup, J.; Immergut, E. H., Eds. "Polymer Handbook"; Wiley: New York, 1975.
(13) Matsuzaki, K.; Kanai, T.; Kawamura, T.; Matsumoto, S. *J. Polym. Sci., Polym. Phys. Ed.* **1973**, *11*, 961.
(14) Farrar, T. C.; Becker, E. D. "Pulse and Fourier Transform NMR"; Academic Press: New York, 1971.
(15) Abragam, A. "Principles of Nuclear Magnetism"; Clarendon Press: Oxford, 1962.
(16) Jones, A. A.; Stockmayer, W. H. *J. Polym. Sci., Polym. Phys. Ed.* **1977**, *15*, 847.
(17) Lyerla, J. R.; Horikawa, T. T.; Johnson, D. E. *J. Am. Chem. Soc.* **1977**, *99*, 2463.
(18) Asakura, T.; Doi, Y. *Macromolecules* **1983**, *16*, 786.
(19) Inoue, Y.; Nishioka, A.; Chujo, R. *J. Polym. Sci., Polym. Phys. Ed.* **1973**, *11*, 2237.
(20) Grandjean, J.; Sillescu, H.; Willenverg, B. *Makromol. Chem.* **1977**, *178*, 145.
(21) Adriansens, G. J.; Bjorkstan, J. L. *J. Chem. Phys.* **1972**, *56*, 1123.
(22) Mashimo, S.; Winsor, P.; Cole, R.; Matso, K.; Stockmayer, W. H. *Macromolecules* **1983**, *16*, 965.
(23) Jelinski, L. W.; Dumais, J. J.; Engel, A. K. *Macromolecules* **1983**, *16*, 492.
(24) Skolnick, J.; Helfand, E. *J. Chem. Phys.* **1980**, *72*, 5489.
(25) Levy, G. C.; Axelson, D. E.; Schwartz, R.; Hochmann, J. *J. Am. Chem. Soc.* **1978**, *100*, 410.
(26) Heatley, F.; Cox, M. *Polymer* **1977**, *18*, 399.
(27) Cohen-Addad, J. P.; Guillermo, A.; Messa, J. P. *Polymer* **1979**, *20*, 536.
(28) Cohen-Addad, J. P. *J. Chem. Phys.* **1979**, *71*, 3689.
(29) Ferry, J. D. "Viscoelastic Properties of Polymers"; Wiley: New York, 1983.
(30) Turnbull, D.; Cohen, M. H. *J. Chem. Phys.* **1961**, *34*, 120.
(31) Cohen-Addad, J. P.; Faure, J. P. *J. Chem. Phys.* **1974**, *61*, 1571.
(32) We have also fit our data to the model of Hall and Helfand (*J. Chem. Phys.* **1982**, *77*, 3275) using the spectral density reported by Connolly et al. (*Macromolecules*, **1984**, *17*, 722). The results were deemed nonphysical and this was probably due to the different frequencies of motion associated with T_1 and T_2. The Hall–Helfand model is specifically derived for very short-range motions and apparently cannot accommodate the longer range motions to which the T_2 is sensitive.

A General Linear-Viscoelastic Theory for Nearly Monodisperse Flexible Linear Polymer Melts and Concentrated Solutions and Comparison of Theory and Experiment

Y.-H. Lin

Exxon Chemical Company, Plastics Technology Division, Baytown, Texas 77522.
Received March 13, 1984

ABSTRACT: Rheological properties are much related to the molecular dynamics in concentrated polymer systems. The reptational chain model of Doi and Edwards has successfully explained many characteristic features of viscoelasticity of flexible linear polymers. The Doi–Edwards theory predicts that the zero-shear viscosity scales with molecular weight, M, as $\eta_0 \propto M^3$ while the well-known experimental result is $\eta_0 \propto M^{3.4}$. This discrepancy is a fundamental pending problem associated with the molecular theory. We have theoretically identified four modes of polymer dynamics: the Rouse motion between two entanglement points, the chain slippage through entanglement links, the chain contour length fluctuation, and the chain reptational motion corrected for the chain length fluctuation effect. Including all these four dynamic modes, a general functional form for the stress relaxation modulus after a step shear deformation in the linear region has been derived. Extensive and consistent agreements between theory and experiment have been obtained. The theory allows the analysis of the entire linear viscoelastic spectrum and explains (a) the 3.4 power law of viscosity as a function of molecular weight, (b) the molecular weight dependence of steady-state compliance, (c) the transition point of viscosity, M_c, and (d) the transition point of the steady-state compliance M_c'. We have used the theory "literally" in analyzing experimental data. The consistency observed in the agreements of theory and experiment may allow for exact definition of several fundamental physical quantities in polymer dynamics and viscoelasticity.

I. Introduction

Linear viscoelasticity of polymers is a very important aspect of rheological study. On one hand it is closely related to the molecular structure (molecular weight (MW), molecular weight distribution (MWD), and long branches),[1] and on the other hand it determines the relaxation of polymer stress or orientation in processing.[2,3] Thus, it plays an essential role in linking polymer structure and processing. Despite its importance, a completely good understanding of its relation with molecular structure has been lacking even for the simplest cases such as flexible linear polymers of very narrow MWD.

In 1971, de Gennes[4] described the diffusion of a linear polymer molecule in a network system as reptation in a "tube". In 1978, Doe and Edwards[5-8] recognized the important relation of the reptational motion and the me-

0024-9297/84/2217-2846$01.50/0

chanical properties of a concentrated polymer system. In their series of publications, a rheological constitutive equation was derived by considering the motion of a single polymer molecule in the mean field imposed by the other chains. Their theory has successfully explained many characteristic features of viscoelasticity of concentrated polymer systems.

The Doi–Edwards theory predicts that the zero-shear viscosity scales with molecular weight, M, as $\eta_0 \propto M^3$. The well-known experimental result is $\eta_0 \propto M^{3.4}$[9] for M above the viscosity transition point, M_c. This discrepancy is a fundamental pending problem associated with the molecular theory. Below M_c, the viscosity increases with M as predicted by the Rouse theory.[10] Empirically, the value of M_c is about twice the entanglement molecular weight, M_e (the molecular weight of the polymer chain between two entanglement points).[1,11]

Since the Rouse theory considers only the *intramolecular* motions while the Doi–Edwards theory deals with the *intermolecular* interaction (entanglement) and its relaxation by reptational motion (diffusion) of the polymer molecule without taking any intramolecular motion into account, some sort of "gap" is expected to exist between these two theories. Therefore, some sort of intramolecular motion need be incorporated into the Doi–Edwards theory to make a continuous transition from the reptational regime to the Rouse regime. Doi[12,13] introduced an additional motion: fluctuation of the primitive chain length. Due to the fluctuation, the chain moves in and out of the tube and relaxes the stress at both tube ends. He showed that this mechanism could account for the difference between $\eta_0 \propto M^{3.4}$ (experiment) and $\eta_0 \propto M^3$ (Doi–Edwards).

Considering several basic assumptions of the tube model that have been proven quite valid, Doi's mechanism appears very promising. Doi's theoretical results, however, still have several defects.

On the basis of a physical picture similar to that proposed by Doi, we have derived a general stress relaxation function (after a step deformation) in a different way. We have analyzed the measured line shapes of stress relaxation of three very narrow MWD ($M_w/M_n \lesssim 1.1$) polystyrene samples in terms of the derived equation. The MWDs extracted from such analyses are in good agreement with those of GPC.

The stress relaxation function is shown to be general and universal for all flexible linear polymers. The MW dependence of all the static and dynamic quantities can be reduced to the forms expressed in terms of the reduced value MW/M_e.

The zero-shear viscosity and steady-state compliance were calculated as a function of MW from the general theory. Good agreements between theory and experiment have been obtained in a consistent manner from the reptational regime to the Rouse regime. The transition points, M_c and M_c', are thus also well described.

In the region $M < 5M_e$, the contributions of the fast motions (the segmental density equilibration motion and the Rouse motion between two entanglement points) to the zero shear viscosity and steady-state compliance become appreciable. It is also shown that in the region, $M_e < M < M_c$, both theoretical and experimental values are somewhat larger than the free Rouse chain value. The difference is due to the tube effect that still remains in the low MW polymers and the larger transverse friction coefficient.

II. Theory

For a step deformation **E**, Doi and Edwards derived the stress relaxation in the reptational regime (i.e., after a certain segmental density equilibrium time, T_{eq}) as

$$\sigma = \frac{3nkTL}{a}\mathbf{Q}\sum_{p\,\mathrm{odd}}\frac{8}{p^2\pi^2}\exp(-tp^2/\tau_C^\circ) + p\delta \qquad (1)$$

with

$$\mathbf{Q} = \left\langle \frac{(\mathbf{E}\cdot\mathbf{u})(\mathbf{E}\cdot\mathbf{u})}{|\mathbf{E}\cdot\mathbf{u}|} \right\rangle \Big/ \langle|\mathbf{E}\cdot\mathbf{u}|\rangle - \frac{1}{3}\delta \qquad (2)$$

where n is the number of polymer molecules per unit volume, L is the contour length of the primitive chain or the tube, a is the average distance between adjacent entanglement points, k is the Boltzmann constant, $\mathbf{u}$ is a unit vector along the contour of the polymer chain averaged over the fast Rouse motion between two entanglement points, and τ_C° is the longest reptational relaxation time, given as

$$\tau_C^\circ = \frac{L^2}{D\pi^2} = \frac{\zeta b^2}{\pi^2 kT}\frac{N_0^3}{N_e} \qquad (3)$$

where D is the curvilinear diffusion coefficient of the polymer chain in the tube, ζ is the friction coefficient associated with each statistical segment of length b, and N_0 and N_e are numbers of segments per molecular weight and entanglement molecular weight, respectively.

Defining a MW independent constant, K, as

$$K = \frac{\zeta b^2 N_0^2}{kT\pi^2 M^2} \qquad (4)$$

we can rewrite eq 3 as

$$\tau_C^\circ = K\frac{M^3}{M_e} \qquad (5)$$

For a simple shear deformation, the stress relaxation modulus in the linear regime is obtained from eq 1 and 2 as

$$G(t) = \frac{4nkTL}{5a}\mu_C(t/\tau_C^\circ) \qquad (6)$$

with

$$\mu_C(t/\tau_C^\circ) = \sum_{p\,\mathrm{odd}}\frac{8}{p^2\pi^2}\exp(-tp^2/\tau_C^\circ) \qquad (7)$$

The plateau modulus is thus

$$G_N = \frac{4nkTL}{5a} = \frac{4\rho RT}{5M_e} \qquad (8)$$

After a period of T_{eq} following a step deformation, the whole length of the tube is in a deformed state and stress anisotropy is distributed over it. As the time passes, the tube stress will relax through the reptational motion of the polymer chain (eq 1) back and forth inside the tube. In addition to this process, the stress at both tube ends will relax as the primitive chain moves in and out of the tube due to the chain contour length fluctuation $\delta L(t)$.

If the reptational time τ_C° were infinitely long, the only relaxation process would be the fluctuation $\delta L(t)$. Defining the correlation time of $\delta L(t)$ as τ_B, then at $t \simeq \tau_B$, the portion of the tube that still possesses stress will be reduced to a certain length L_0 as shown in Figure 1.

At $t < \tau_B$, the portion of tube possessing stress can be defined as

$$L(t) = L_0 + \overline{\delta L(t)} \qquad (9)$$

Because $\overline{\delta L(t)}$ remains in the original tube, we can consider it as the amount of the fluctuation $\delta L(t)$ that is still cor-

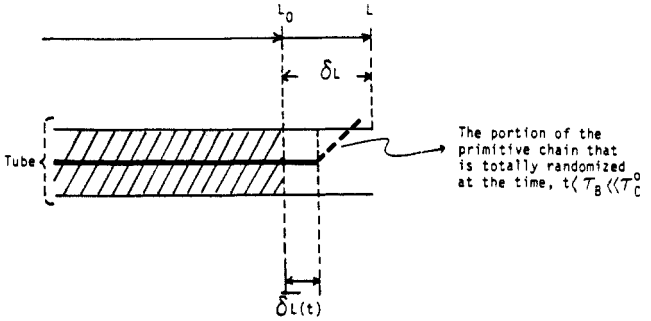

Figure 1. See the text. For simplicity, only one end of the tube is shown.

related with the original value $\delta L(0)$. Thus, we can define $\overline{\delta L(t)}$ as the projection of $\delta L(t)$ to $\delta L(0)$ given as

$$\overline{\delta L(t)} = \frac{\langle \delta L(0)\delta L(t)\rangle}{\langle \delta L(0)^2\rangle^{1/2}} \tag{10}$$

We have derived as shown in the Appendix

$$\overline{\delta L(t)} = (N_0 b^2)^{1/2}\mu_B(t/\tau_B) \tag{11}$$

with

$$\mu_B(t/\tau_B) = \sum_{p\,\mathrm{odd}} \frac{8}{p^2\pi^2} \exp(-tp^2/\tau_B) \tag{12}$$

where

$$\tau_B = \frac{1}{3}KM^2 \tag{13}$$

In reality, τ_C° cannot be infinitely long. In order to keep the form of relaxation given by eq 9, 11, 12, and 13 still valid for finite τ_C°, τ_B would be infinitely short compared to τ_C° for the relaxation of the remaining stress associated with L_0 by means of the reptational motion.

As the chain end reaches a certain point of the tube, the stress on the portion of the tube between the point and the original tube end is relaxed. τ_B is so short that at any instance the chain length would effectively be shortened to L_0 ($=L - \delta L$) as far as the tube stress relaxation is concerned. Therefore, the relaxation time τ_C° need be modified to

$$\tau_C = \frac{L_0^2}{D\pi^2} \tag{14}$$

The diffusion coefficient, D, which is proportional to the number of chain segments of the polymer, is not affected by the fast fluctuation.

Thus, including the relaxations of $\overline{\delta L(t)}$ and L_0 and using the results of eq 9–14, we can rewrite eq 6 as

$$G(t) = \frac{4nkTL}{5a}[B\mu_B(t/\tau_B) + C\mu_C(t/\tau_C)] \tag{15}$$

where as shown in the Appendix

$$B = \frac{\delta L}{L} = (M_e/M)^{1/2} \tag{16}$$

$$C = 1 - B \tag{17}$$

$$\tau_C = K\frac{M^3}{M_e}[1 - (M_e/M)^{1/2}]^2 \tag{18}$$

III. Fast Motions and Plateau Moduli

In addition to the relaxation process $\mu_B(t/\tau_B)$ and $\mu_C(t/\tau_C)$ described above, there are two fast relaxation processes in the short time region of stress relaxation. One is associated with the Rouse motion of the polymer chain between two adjacent entanglement points. For modeling this process, the entanglement points can be assumed as cross-linked points. The solution to this problem was derived long ago.[14] Following Doi's notation,[15] we refer to this process as $\mu_A(t)$ given as

$$\mu_A(t) = \sum_p \exp(-t/\tau_A{}^p) \tag{19}$$

with

$$\tau_A{}^p = \frac{K\pi^2}{24\sin^2(\pi p/2N_e)}\frac{M_e^2}{N_e^2} \tag{20}$$

We have found that the experimental results can be better described if the exact solution given by eq 20 is used. If N_e is very large, eq 20 reduces to the approximate equation given by Doi.[15]

The other relaxation process is related to the slippage of a polymer chain through entanglement links. In the theory of rubber elasticity,[16,17] the plateau stress is given as

$$\sigma = \frac{3\rho RT}{M_e}\mathbf{Q}' + p\delta \tag{21}$$

with

$$\mathbf{Q}' = \langle(\mathbf{E}\cdot\mathbf{u})(\mathbf{E}\cdot\mathbf{u})\rangle - \frac{1}{3}\delta \tag{22}$$

From eq 21 and 22, the plateau modulus for a simple shear is given as

$$G_N' = \frac{\rho RT}{M_e} \tag{23}$$

Equations 8 and 23 differ by a factor of $^4/_5$. We can understand the difference by comparing eq 2 and 22. In eq 2 the $|\mathbf{E}\cdot\mathbf{u}|$ factor inside the first bracket is due to slippage of a polymer chain through entanglement links to achieve an equilibrium segmental density along the chain contour. The $\langle|\mathbf{E}\cdot\mathbf{u}|\rangle$ factor in the denominator is related to the reduction of entanglement density (disentanglement). It can be shown that in the linear regime the disentanglement effect is zero. Thus, we can conclude that the plateau modulus transits from $\rho RT/M_e$ to $4\rho RT/5M_e$ only because the chain slips through the entanglement links to release the unevenness of tension (related to segmental density) along the chain contour. We shall refer to this process as $\mu_X(t)$ with a characteristic relaxation time τ_X. Since the chain slippage motion involves several entanglement segments, while $\mu_A(t)$ is for motions associated with a single entanglement segment and $\mu_B(t)$ with the whole molecule, it is clear that $\tau_B > \tau_X > \tau_A$ and τ_X is equivalent to T_{eq} of Doi and Edwards in the linear regime.

We do not know the relaxation form for $\mu_X(t)$ at this stage. For our analysis of experimental data, we have assumed that it decays single exponentially. Comparing eq 8 and 23, the relaxation strength of $\mu_X(t)$ can be obtained. Including the fast relaxation processes together with the $\mu_B(t/\tau_B)$ and $\mu_C(t/\tau_C)$ processes (eq 15), we write a general equation for the stress relaxation modulus as

$$G(t) = \frac{4\rho RT}{5M_e}[1 + \mu_A(t/\tau_A)]\left[1 + \frac{1}{4}\exp(-t/\tau_X)\right] \times [B\mu_B(t/\tau_B) + C\mu_C(t/\tau_C)] \tag{24}$$

As shown below, eq 24 in combination with eq 12, 13, and 16–20 is used to analyze the measured master curves

of stress relaxation over the whole dynamic range.

IV. Experiment

Polystyrene samples of very narrow MWD ($M_w/M_n \lesssim 1.1$) were used for stress relaxation measurements in this study. The measurements were made with the System Four mechanical spectrometer manufactured by Rheometrics Inc. The details of sample preparation and equipment calibration have been described before.[18]

The polystyrene samples studied: F20 (MW = 186000, M_w/M_n = 1.07), F40 (M_w = 422000, M_w/M_n = 1.05), and F80 (M_w = 775000, M_w/M_n = 1.01) were obtained from and characterized by TSK (Toyo Soda Manufacturing Co., Japan). Because the M_w of F80 is too high for feasible stress relaxation measurement at low temperature (~135 °C), enough measurements were made only on F20 and F40 for making their master curves.

In this study, the shifting factors in making the master curves would affect our data analysis very much. Careful procedures have been taken to determine the shifting factors. The regions of the stress relaxation curves, which have substantial change in both modulus and time axes, were used for overlapping. Thus, the plateau region was avoided. The shifting factors based on the overlapping are obtained through computer fitting.

V. Line Shape Analysis of Stress Relaxation Curves

Effect of Molecular Weight Distribution. Equation 24 as well as the Doi–Edwards theory are only applicable for ideally monodisperse polymers. Because the reptational relaxation time τ_C is highly sensitive to molecular weight (eq 18), the effect of the finite MWD need be taken into account even for polymers of very narrow MWD ($M_w/M_n \lesssim 1.1$). It has been shown that failure to do so can be misleading as in the assessment of the tension coefficient[18,19] that occurs in the theory of Curtiss and Bird.[20,21]

If the MWD is very narrow ($M_w/M_n \lesssim 1.1$), the linear additivity of the contribution from each molecular weight component is valid. If the MWD is broad, a certain nonlinear blending law is required.[22] For a narrow MWD, we have shown[18] that a composition of several discrete MW components can approximate a certain continuous MWD function for stress relaxation curve calculation. As far as the M_w/M_n value of the polymer is concerned, the two MWD's, discrete and continuous, are equivalent. Here, for simplifying the computation, we have used the discrete distribution. We have found that assuming three components for the distribution is sufficient to analyze all our data.

Computer Fitting Procedure. In the nonlinear least-squares fitting procedures, we have separated the stress relaxation curve into two sections: one mainly contains the $\mu_B(t)$ and $\mu_C(t)$ processes and the other includes the $\mu_A(t)$ and $\mu_X(t)$ processes in the short time region. First, we fitted the portion of stress relaxation data containing only the $\mu_B(t)$ and $\mu_C(t)$ processes in the long time region to eq 15 with K, and the MW's and amplitudes (i.e., the contributions to the total plateau modulus from the discrete MW components, which are proportional to weight fractions) of the three components of the assumed MWD as adjustable parameters. During the fitting the weight-averaged MW of the three-component MWD was fixed at the predetermined value of the sample (i.e., the value of the sample as characterized by TSK).

The obtained best values of the fitting parameters were then used as known values in eq 24 to do the nonlinear least-squares fitting for the $\mu_A(t)$ and $\mu_X(t)$ processes with N_e, K' (K of eq 20), and τ_X as adjustable parameters. It was found that N_e = 10 gave the best fitting results in the short time region as shown below. The obtained best values of N_e, K', and τ_X were then put into eq 24 to repeat

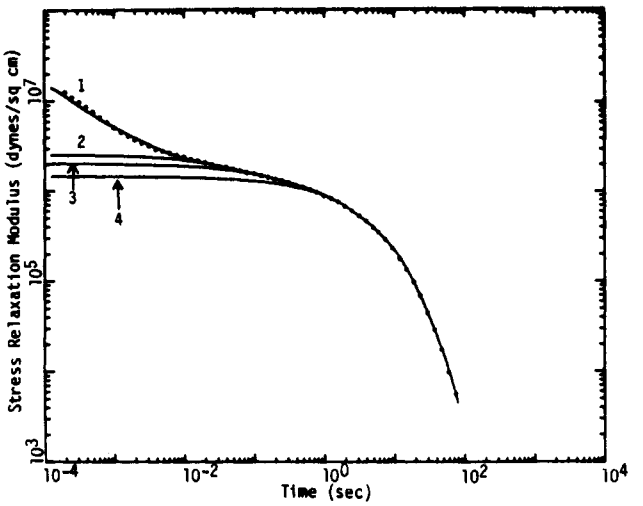

Figure 2. Comparison of the experimental stress relaxation master curve (dots) and the theoretical curve calculated using the MWD shown in Figure 4 for F20. Also shown are the separate contributions from $\mu_A(t)$ (line 1), $\mu_X(t)$ (line 2), $\mu_B(t)$ (line 3), and $\mu_C(t)$ (line 4).

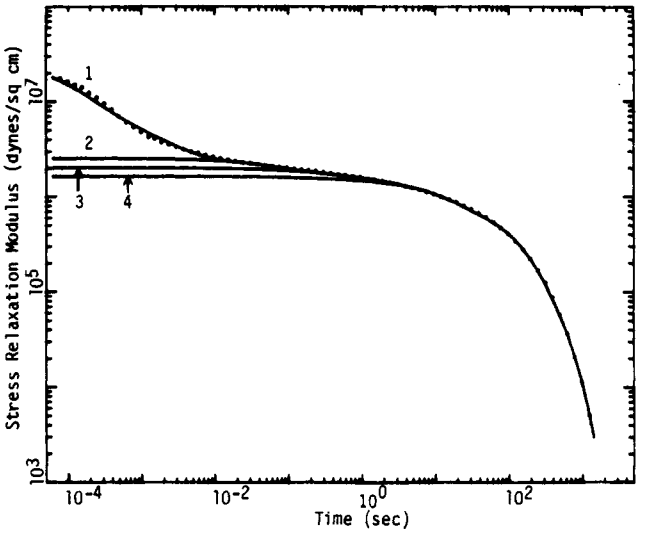

Figure 3. Same as Figure 2 for F40. The MWD is shown in Figure 5.

the nonlinear least-squares fitting for the $\mu_B(t)$ and $\mu_C(t)$ processes over a wider range than initially considered in using eq 15. This eliminated the initial arbitrariness for picking a first datum point for doing the least-squares fitting to the $\mu_B(t)$ and $\mu_C(t)$ processes. We repeated this fitting procedure until the values of the parameters did not change further.

Entanglement Molecular Weight, M_e. The value of M_e used in the computer calculation is obtained by a separate procedure from the fitting procedure described above. Initially, a proper M_e value is assumed to do the nonlinear least-squares fitting as described above. The plateau modulus obtained from the computer fitting is then used to calculate the M_e value according to eq 8. The assumed M_e value is then compared with the calculated value and adjusted accordingly until a consistency between the assumed and the calculated is obtained.

Results of Analysis. The stress relaxation curves of F20 and F40 were measured at different temperatures. Their master curve were obtained at 154 ± 1 °C by the procedure described in section IV. The experimental and calculated stress relaxation curves are shown together in Figures 2 and 3 for F20 and F40, respectively. The obtained three-component MWD's from the least-squares

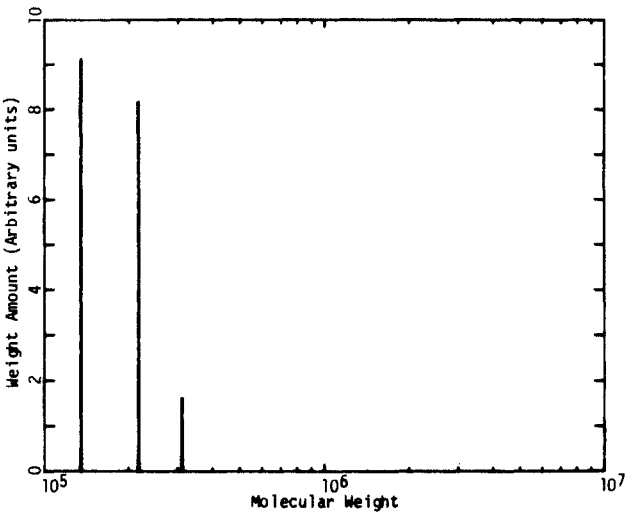

Figure 4. Three-component MWD of F20 extracted from analyzing the stress relaxation data (see Figure 2).

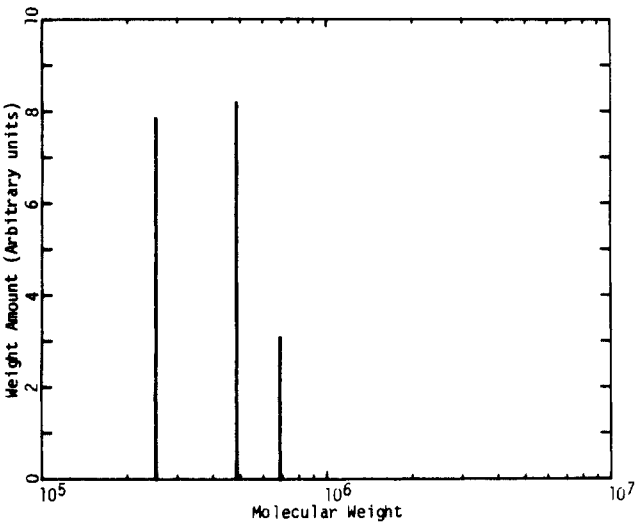

Figure 5. Same as Figure 4 for F40 (see Figure 3).

fittings are shown in Figures 4 and 5. The M_w/M_n values calculated from these distributions are 1.08 for F20 and 1.15 for F40. These values agree well with those of GPC.

In Figures 2 and 3, the calculated separate contributions from $\mu_A(t)$, $\mu_X(t)$, $\mu_B(t)$, and $\mu_C(t)$ are also shown. It is quite clear that in the short time region, the polymer dynamics is basically the Rouse motion between two fixed points. In the plateau region, the decline of stress level is largely due to the $\mu_B(t)$ process. Comparing Figures 2 and 3, one can notice that the contribution of $\mu_B(t)$ is greater at lower MW. This is so because of eq 16. As shown below this has much to do with the deviation of the experimental observation $\eta_0 \propto M^{3.4}$ from $\eta \propto M^3$ of the Doi–Edwards theory. Between $\mu_A(t)$ and $\mu_B(t)$, a transition region exists as described by $\mu_X(t)$. Presently, we do not know the relaxation form for $\mu_X(t)$ and have assumed a single exponential form for it.

For F20 and F40 at 154 °C, we have obtained the best values listed in Table I for the fitting parameters: G_N, M_e, and K. Despite the higher declining rate of the stress in the plateau region for F20, we have extracted out the same value of the plateau modulus for F20 as for F40. This suggests that we can properly analyze the data in terms of eq 24. The calculated and assumed M_e values are in good agreement with that obtained from multiplying the factor $^4/_5$ to the value, M_e = 17 300, obtained by D. J. Plazek et al. according to eq 23 at 140 °C. Most importantly, the K values are the same within experimental error for both F20 and F40. This indicates that eq 13 and 18 have the right MW dependence for τ_B and τ_C, respectively.

Table I
Best Values for the Fitting Parameters G_N, M_e, and K from Analyzing the Stress Relaxation Master Curves of F20 and F40 at 154 ± 1 °C

	F20	F40
G_N	205 × 10^4 (dyn/cm^2)	206 × 10^4 (dyn/cm^2)
M_e	13 800 (assumed) 13 700 (calcd)	13 800 (assumed) 13 700 (calcd)
K	1.8 × 10^{-11}	1.9 × 10^{-11}

Table II
Best Values for the Fitting Parameters G_N, M_e, and K from Analyzing the Stress Relaxation Curves of F40 and F80 at 185 ± 1 °C

	F40	F80
G_N	229 × 10^4 (dyn/cm^2)	224 × 10^4 (dyn/cm^2)
M_e	13 000 (assumed) 12 900 (calcd)	13 000 (assumed) 13 200 (calcd)
K^a	0.49 × 10^{-12}	0.47 × 10^{-12}

[a] Our sample temperature control can drift about 1 °C from day to day. These numbers for K are the average values of three sets of samples; each set was measured during the same day. These values are (F40 vs. F80) 0.47 vs. 0.48, 0.42 vs. 0.40, and 0.59 vs. 0.53.

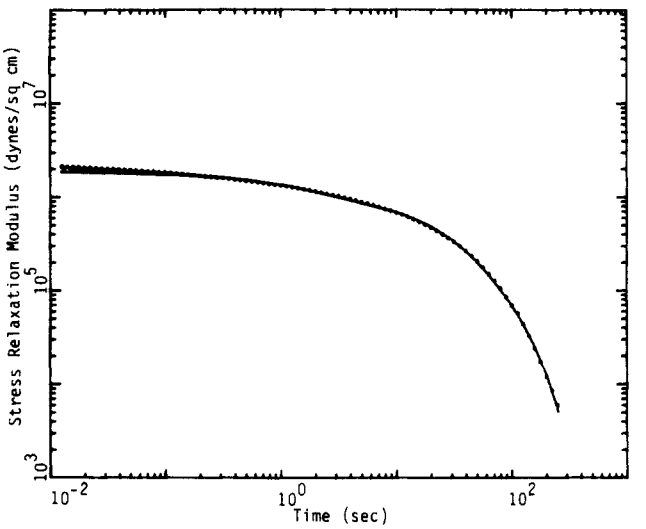

Figure 6. Comparison of the experimental stress relaxation data (dots) and the theoretical curve calculated using the MWD for F80 shown in Figure 7. The tail of the $\mu_B(t/\tau_B)$ relaxation is also shown.

To confirm the MW dependence of τ_B and τ_C as given by eq 13 and 18, we made the stree relaxation measurements of F40 and F80 under the same conditions at 185 ± 1 °C. Because of the limit of the time window of the stree relaxation measurement for F80, the analysis of the data was only carried out in the terminal region. This is sufficient to determine the G_N and K values. The experimental and calculated relaxation curves of F80 are shown together in Figure 6. The obtained best values for the fitting parameters for both F40 and F80 at 185 °C are shown in Table II.

These results confirm what we have concluded from Table I. K is independent of MW, and quite consistently eq 13 and 18 provide the MW dependence for τ_B and τ_C. This will be further supported by our analysis of viscosity data as a function of MW as described below.

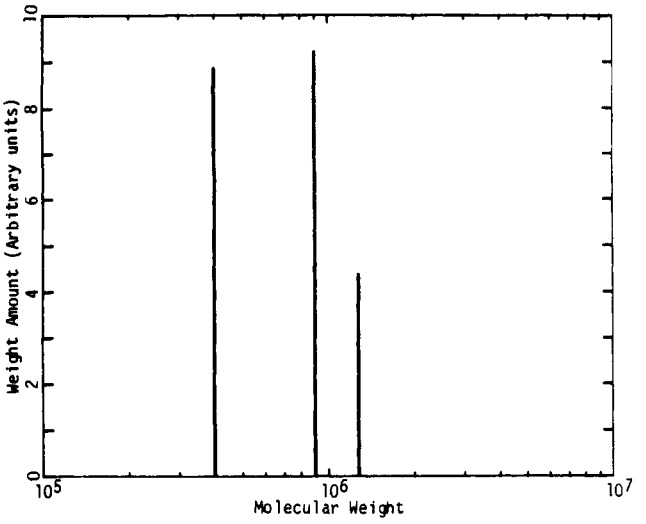

Figure 7. Same as Figure 4 for F80 (see Figure 6).

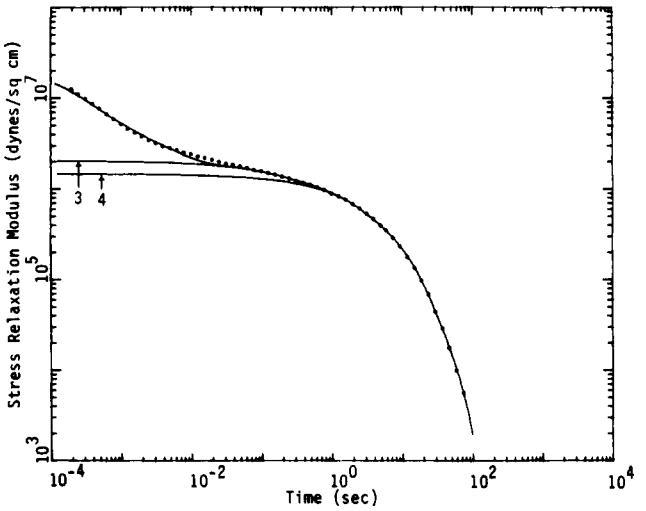

Figure 8. Comparison of the experimental stress relaxation master curve (dots) and the theoretical curve calculated without the $\mu_X(t)$ process for the F20 sample (compare with Figure 2).

Shown in Figure 7 is the MWD for F80 obtained from the least-squares fitting. The M_w/M_n value calculated from the MWD is 1.24, which is somewhat higher than the GPC value ($M_w/M_n = 1.01$). Comparing the results of F20, F40, and F80, we have observed a trend of increasing calculated M_w/M_n value with increasing M_w. An explanation for the trend based on the mechanism of anionic polymerization of these samples is given below.

$\mu_A(t)$ and $\mu_X(t)$ Processes. According to the model of Doi and Edwards, the $\mu_X(t)$ process exists for a polymer melt. For comparison with Figures 2 and 3, the analysis of the relaxation master curves of F20 and F40 without the $\mu_X(t)$ process in the relaxation functional form (i.e., the second bracket of eq 24 is set equal to 1) is shown in Figures 8 and 9, respectively.

Without including $\mu_X(t)$ in the data analysis, the region between the $\mu_A(t)$ and $\mu_B(t)$ relaxations cannot be properly described. Several experimental results[18,23,24] have shown that eq 2 correctly describes the nonlinear rheological effect (the so called damping function). Therefore, the observation of the $\mu_X(t)$ process is a logical consequence of the valid description of chain slippage through entanglement links by Doi and Edwards.

In the shorter time region than the polymer chain has a chance to slip through an entanglement link, the polymer dynamics is basically the Rouse motion between two fixed points. For better analyzing the stress relaxation data in this region, we used the exact solution given by eq 20 instead of the approximate form as given by Doi.[15] This is quite reasonable, since considering the M_e value, the number of statistical Kuhn segments between two adjacent entanglement points cannot be very large. To illustrate this point, we show in Figure 10 the stress relaxation master curve of F40 analyzed using the approximate form for τ_A^p for comparison with Figure 3.

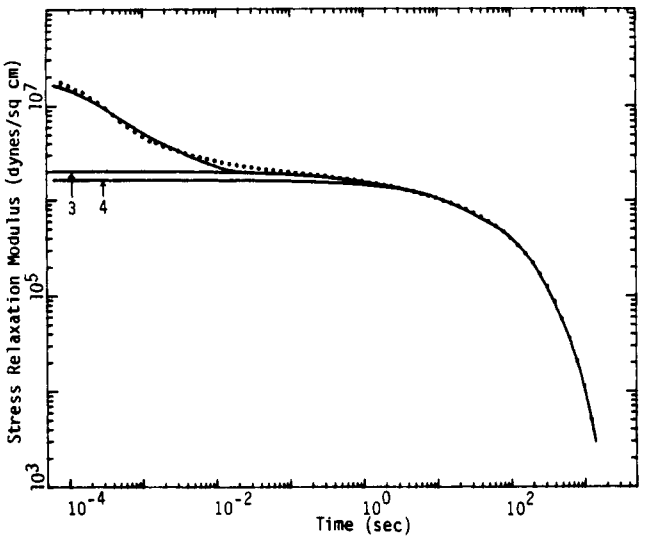

Figure 9. Same as Figure 8 for the F40 sample (compare with Figure 3).

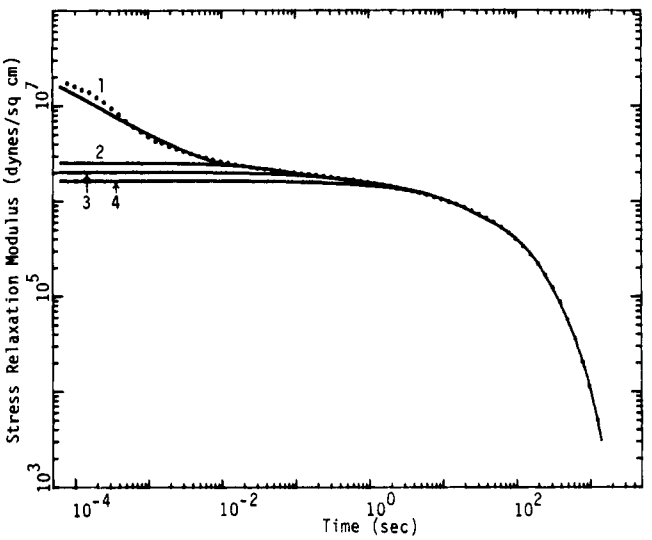

Figure 10. Comparison of the experimental stress relaxation master curve (dots) and the theoretical curve calculated using the approximate form for the $\mu_A(t)$ process for the F40 sample (compare with Figure 3).

As expected, the K' values (i.e., the K value of eq 20) obtained from the analysis of the $\mu_A(t)$ relaxation processes of F20 and F40 are the same within the experimental error (9.6×10^{-11} for F20 and 9.3×10^{-11} for F40). However, the K' values are about five times the K values. Examining eq 20, there are two possible ways to explain the difference. First, one can think that the effective M_e value in the $\mu_A(t)$ region is about $5^{1/2}$ times the M_e value applicable in the long time region, because an entanglement link is not as tight as a cross-linked point. Such an explanation causes an inconsistency between the definitions of the plateau modulus, G_N, and the initial modulus of the $\mu_A(t)$ process. The remaining possible explanation is to attribute the larger K' value to the larger friction coefficient for the Kuhn segment to move in the direction perpendicular to

the primitive chain contour.[15] As shown below, the calculated zero-shear viscosity and steady-state compliance values based on this explanation are in good agreement with the experimental values.

VI. Universality of the Stress Relaxation Function

Considering the chain contour length fluctuation, the Doi–Edwards theory is modified to give a stress relaxation function containing the $\mu_B(t)$ and $\mu_C(t)$ processes. Including the fast motions: $\mu_A(t)$ and $\mu_X(t)$ processes, a general stress relaxation function (eq 24) is obtained.

The theory is universal and should be applicable to all flexible linear homopolymers. All the static (B and C, see eq 16 and 17) and dynamic (τ_B/τ_A and τ_C/τ_A, see eq 13, 18 and 20) quantities are expressed in terms of the reduced MW: M/M_e. The M_e value is determined from the plateau modulus, G_N, according to eq 8.

Without knowing the exact relaxation form for $\mu_X(t)$, we have not discerned the MW dependence of τ_X. We can, however, obtain some understanding about the $\mu_X(t)$ process through scaling.

Assume

$$\tau_X \propto M^m \tag{25}$$

where m is some number greater than zero and smaller than 2 (τ_X should not have as strong a MW dependence as τ_B).

For keeping the universality of the stress relaxation function applicable in the $\mu_X(t)$ region, τ_X/τ_A should be a function of the reduced MW, M/M_e only. This requires

$$\tau_X \propto M_e^{2-m}M^m \tag{26}$$

From our data analysis, the obtained τ_X values = 0.027 for F20 and 0.058 for F40 at 154 °C are closely proportional to the MW's of the samples, i.e., $m = 1$.

This suggests that the reduced time constant, τ_X/τ_A, is proportional to the number of entanglement links on the molecule or the reduced MW, M/M_e, and that

$$\tau_X \approx KM_eM \tag{27}$$

Using the known M_e value, the weight-averaged MW values for M and the K values listed in Table I, we have estimated $\tau_X \approx 0.046$ for F20 and $\tau_X \approx 0.11$ for F40. These values compare very favorably with the values extracted from the data analysis for $\mu_X(t)$ in terms of a single exponential form. This supports the universality of the stress relaxation form, eq 24, extending over the whole dynamic range.

VII. Zero-Shear Viscosity

In linear viscoelasticity, the zero-shear viscosity, η_0, is related to the stress relaxation modulus, $G(t)$, as

$$\eta_0 = \int_0^\infty G(t)\,dt \tag{28}$$

Both $\mu_A(t)$ and $\mu_X(t)$ relax much faster than $\mu_C(t)$. Firstly, we assume that their contributions to η_0 is negligible. Substituting eq 15 into eq 28, we have obtained

$$\eta_0 = \frac{\rho RT\pi^2}{15}K\frac{M^3}{M_e^2}\left[(1-(M_e/M)^{1/2})^3 + \frac{1}{3}(M_e/M)^{1.5}\right] \tag{29}$$

This equation differs somewhat from the following equation of Doi.[12]

$$\eta_0 = \frac{\rho RT}{3}K\frac{M^3}{M_e^2}\left[(1-(M_e/M)^{1/2})^3 + \frac{1}{5}(M_e/M)^{1.5}\right] \tag{30}$$

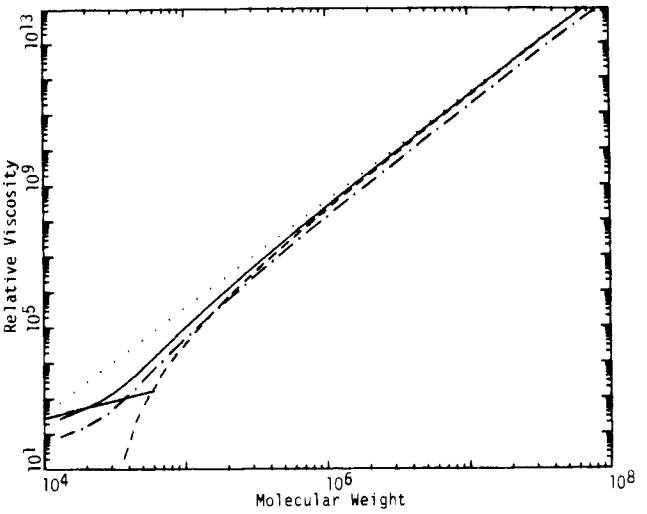

Figure 11. Comparison of the theoretical viscosity curves: Rouse (—) ($M < M_c$), eq 29 (—) ($M > M_c$), Doi Edwards (···), and eq 30 (-··-) and eq 31 (---) of Doi.

Between eq 29 and 30, the proportional constants in the front are different; the proportional constants of the second term inside the bracket are also different.

More recently,[13] Doi gave another equation

$$\eta_0 = \frac{\rho RT\pi^2}{15}K\frac{M^3}{M_e^2}(1-1.47(M_e/M)^{1/2})^3 \tag{31}$$

The main difference of this equation from eq 29 is the lack of the second term.

According to the Rouse theory, the viscosity at low MW is given as

$$\eta_0 = \frac{\rho RT\pi^2}{36}KM \tag{32}$$

For comparison, using the same M_e and K values, we plot out in Figure 11 the calculated values based on eq 29, the Doi–Edwards theory, eq 30 and 31 of Doi, and eq 32. The present equation converges with that of Doi and Edwards in the high MW limit. Equation 30 does not converge with the Doi–Edwards theory. Theoretically, this makes eq 30 somewhat defective, since the chain end effect should become negligible as the MW is very high.

Although eq 31 converges with the Doi–Edwards theory in the high MW limit, as shown in Figure 11 it does not describe the molecular weight dependence of viscosity in the region where most experimental values have been obtained (i.e., in the region where $\eta_0 \propto M^{3.4}$).

Equation 29 crosses eq 32 at $M \sim 1.5\,M_e$. This crossing point should have no direct relation with M_c, as we have noticed that the fast motions: $\mu_A(t)$ and $\mu_X(t)$ processes contribute quite appreciably to the zero shear viscosity for $M < 5M_e$. We calculate the viscosity values as a function of MW from integrating numerically eq 24 using the relations given by equations 12, 13, 16–20, and 27. In the calculation, the experimenatl value for K', which is 5 times the K value, is used in eq 20. And eq 27 is substituted by

$$\tau_X = 0.55KM_eM \tag{33}$$

where the constant, 0.55, is an empirical value (see section VI).

As shown in Figure 12, the integration values converge with values of eq 29 for high MW ($M > 7M_e$) as expected.

Also shown in Figure 12 is the experimental values obtained by Plazek et al.[25] at 160 °C. These experimental data have been corrected for the MW dependence of T_g. The theoretical curves were calculated with M_e = 13 600

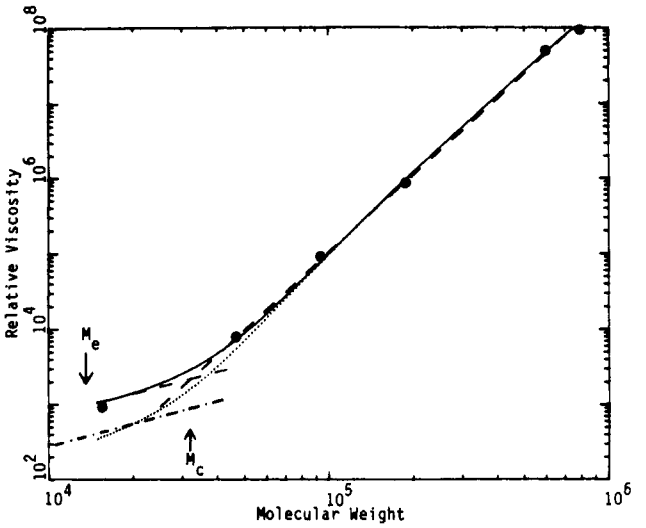

Figure 12. Comparison of the viscosity data of Plazek et al. at 160 °C and the theoretical curves of the numerical integration (see the text) (—), eq 29 (···), and free Rouse chain (- · -). (M_e = 13 600 used in the calculation). Above M_c, the dash line has a slope of 3.4; below M_c, the dash line has a slope of 1.

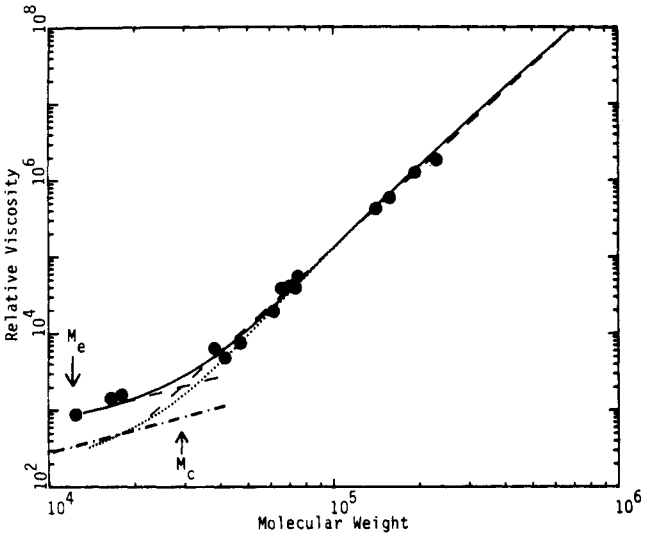

Figure 13. Comparison of the viscosity data of Allen and Fox at 217 °C and the theoretical curves (same as in Figure 12, M_e = 12 200).

for 160 °C. We estimated the M_e value from the values at 185 and 154 °C, which had been obtained from analyzing the stress relaxation data. (Tables I and II) In comparing the theoretical and experimanetal values, we allowed the experimental values to shift along the viscosity coordinate. In other words, K is the only adjustable parameter.

Shown in Figure 13 is a similar comparison of theoretical values and experimental data obtained by Allen and Fox at 217 °C.[26] The correction for the MW dependence of T_g of these experimental values was based on the T_g information of Plazek. The M_e value used in the calculation is 12 200. This value estimated from extrapolation may not be exact. A small difference in the M_e value would not change very much the shape of the curve of η_0 vs. M.

As noticeable in Figures 12 and 13, the integration viscosity values agree with the experimental data very well over the entire MW range. In the low-MW region ($M \gtrsim M_e$), the integration value is apparently proportional to MW. In the high-MW region ($M > M_c$), the integration value as a function of MW can be extremely closely approximated by a line of slope 3.4 as shown in these figures.

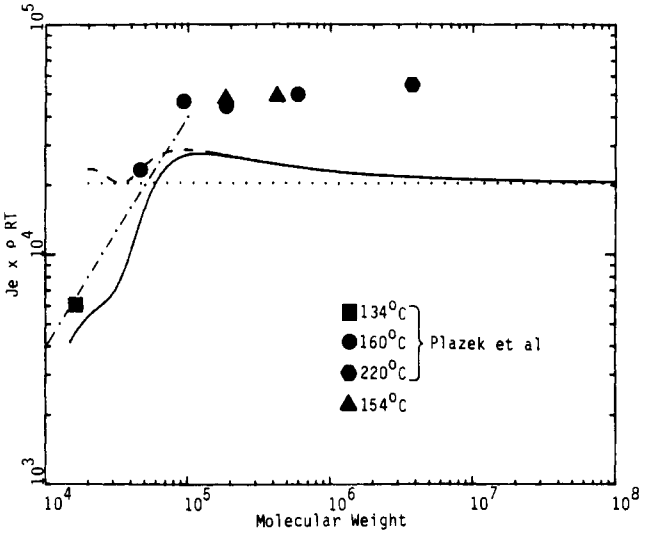

Figure 14. Comparison of the steady-state compliance data and the theoretical curves of Doi–Edwards (···), free Rouse chain (- · -), eq 35 (- - -) and numerical integration (—) (see the text).

Furthermore, the lines of slope 3.4 in the high-MW region and of slope 1 in the low-MW region intersect at MW very close to the M_c literature value.[1,11]

We can also notice that in the low-MW region ($M < M_c$) both the integration and experimental values are about twice higher than the free Rouse values as also shown in Figures 12 and 13. This suggests that the entanglement constraint (the tube effect) still exists in the $M_e < M < M_c$ region.

The larger friction coefficient in the transverse direction also contributes a large part to the higher viscosity value than the free Rouse value. The larger transferse friction coefficient may reflect some local structural correlation between neighboring (intermolecular) Kuhn segments. Since the basis segment is the Kuhn segment, the local structural correlation should be the same for all flexible linear polymer. In other words, the stress relaxation function should also be universal in the $\mu_A(t)$ region.

VIII. Steady-State Compliance

Another important linear viscoelastic quantity for comparison with the theory is the steady-state compliance, J_e, which is given as

$$J_e = \frac{\int_0^\infty tG(t)\,dt}{{\eta_0}^2} \tag{34}$$

Neglecting the contributions of the $\mu_A(t)$ and $\mu_X(t)$ processes, and substituting eq 15 into eq 34, we have obtained

$$J_e = \frac{3M_e}{2\rho RT} \frac{\left[(1-(M_e/M)^{1/2})^5 + \frac{1}{9}(M_e/M)^{2.5}\right]}{\left[(1-(M_e/M)^{1/2})^3 + \frac{1}{3}(M_e/M)^{1.5}\right]^2} \tag{35}$$

J_e was also calculated by numerical integration using eq 24 in eq 34. In the calculation, the values of parameters used are the same as in the case of viscosity calculation. The results are shown in Figure 14 together with the calculated values of eq 35 and the free Rouse chain value. The integration value converges with eq 35 at MW > $10M_e$ and exhibits a maximum around $10M_e$. In the low MW region, the integration value is lower than the free Rouse chain value. Around M_c, the integration value has a

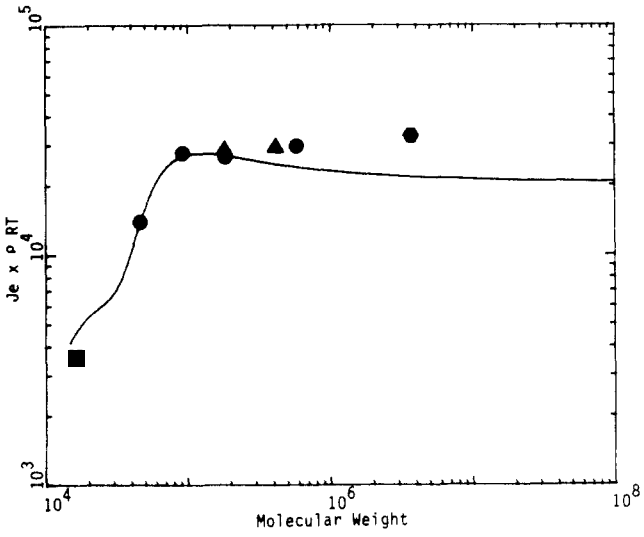

Figure 15. Experimental values of steady-state compliance multiplied by 0.6 for correcting contribution from MWD and compared with the numerical integration values (curve).

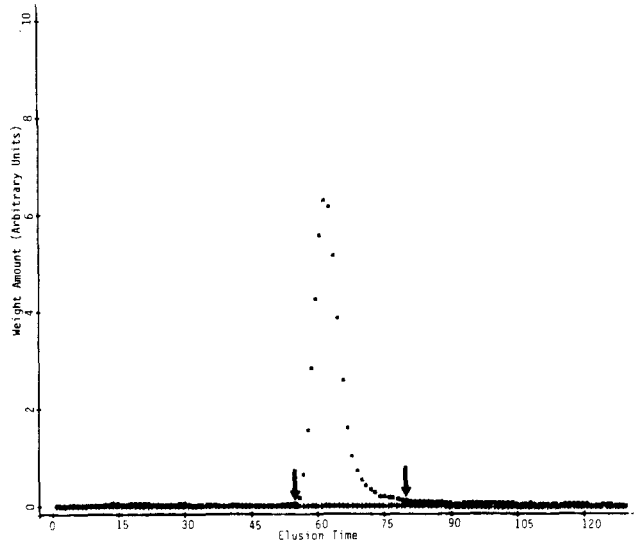

Figure 16. GPC spectrum of the F80 sample MWD between the two arrow pointers has M_w/M_n = 1.08. The long tail on the low-MW side has 7% of the total area.

"bending" point, which appears related to the level-off of viscosity at low MW ($M < M_c$).

For comparison with the theory shown in Figure 14 are also the experimental values of Plazek et al.[25] and the values obtained from the stress relaxation measurements of F20 and F40. The experimental values are larger than the integration values over the entire MW range. All the theoretical curves shown in Figure 14 are based on ideal monodispersity. We have already shown that the stress relaxation data can be well analyzed if the MWD is taken into account. Therefore, the difference between experimental and theoretical values shown in Figure 14 can be attributed to MWD.

Empirically, we multiplied the experimental values by 0.6 to account for the contribution of MWD and compared the results with the integration values in Figure 15. Around the transition region ($3M_e$–$14M_e$), the agreement is very good. In other words, the integration curve correctly predicts the transition point, M_c', for J_e. The "bending" of the integration J_e value around M_c should be smoothed out by the effect of MWD. The $0.6J_e$ value of the lowest MW experimental point appears lower than the theoretical curve. This may be due to the overcorrection of multiplying J_e by 0.6 because the polymer dynamics is more Rouse-like in the low-MW region ($<2M_e$). In the high-MW region ($>14M_e$), the $0.6J_e$ values are somewhat higher than the theoretical values. This indicates that MWD is broader for higher MW samples and is expected from our analysis of stress relaxation data of F20, F40, and F80, where we have observed the same trend of change of MWD with MW.

This is very likely so because, in anionic polymerization, impurity can leave a tail of low MW polymers behind as the weight-averaged MW increases. The tail extends longer, if the MW is higher. The tail may not be included in the calculation of M_w/M_n. Thus, the GPC M_w/M_n values provided by TSK are smaller at higher MW's contrary to most experience. Furthermore, the tail will contribute most to the decline of stress in the plateau region of the measured $G(t)$; this effectively broadens the MWD from the data analysis. ($\Delta t/\Delta G$ is large in the plateau region.)

We have made a separate GPC measurement of the F80 sample. The result is shown in Figure 16. If the distribution data between the two arrow pointers in the figure are used in the calculation of MWD, then $M_w = 7.6 \times 10^5$ and M_w/M_n = 1.08. Most importantly, a tail of about 7% of the total amount extends over a large range on the low MW side. The low MW components can cause a decline of the plateau modulus as much as 14%.[22] This result supports our explanation for the greater MWD extracted out of the analysis of $G(t)$ for the higher MW sample.

IX. Discussion and Conclusion

Intramolecular Motions. In their papers,[5-8] Doi and Edwards mainly dealt with the reptational motion that occurs in the terminal region. After an equilibrium time, T_{eq}, in a step strain stress relaxation, the reptational motion they considered had a fixed chain contour length.

Considering the primitive chain length fluctuation proposed by Doi, we have derived the relaxation form for the $\mu_B(t)$ process, which is responsible for the most part of the stress decline in the plateau region. In the terminal region, the reptational motion is modified because of the same chain length fluctuation effect. Furthermore, we have identified the $\mu_X(t)$ process that exists in the Doi–Edwards theory implicitly. In the short time region, the Mooney's equation for the $\mu_A(t)$ process is used. Including all these four dynamic processes, a general stress relaxation function is obtained.

In terms of the obtained functional form, the stress relaxation curves of three polystyrene samples were analyzed. A very good overall agreement between experiment and theory has been obtained. From the line-shape analysis, we have (a) extracted very reasonable M_w/M_n values for the studied samples compared to the GPC values, (b) shown that the M_e value involved in both $\mu_B(t)$ and $\mu_C(t)$ dynamic processes is consistent with that determined from G_N, and (c) shown that K is independent of MW and thus that eq 13 and 18 provide the MW dependence for τ_B and τ_C.

The decline of stress in the plateau region is largely due to the $\mu_B(t)$ process. The contribution of the $\mu_B(t)$ process is greater at lower MW. Furthermore, the ratio, τ_C/τ_B, obtained from eq 13 and 18 as

$$\tau_C/\tau_B = 3\frac{M}{M_e}[1 - (M_e/M)^{1/2}]^2 \qquad (36)$$

decreases with decreasing MW. In other words, the $\mu_B(t)$ process is closer in time to the $\mu_C(t)$ process at lower MW. These two effects of $\mu_B(t)$ explain why a terminal region is hardly observable for a MW which is only a few times

of the M_e value. These effects of $\mu_B(t)$ and the MW dependence of τ_C (eq 18) are the major factors responsible for the deviation of the experimental observation $\eta_0 \propto M^{3.4}$ from $\eta_0 \propto M^3$ of the Doi-Edwards theory.

To show the universality of eq 24 as applied to linear viscoelastic properties of flexible linear homopolymers, all the relaxation times: τ_X, τ_B, and τ_C are normalized with respect to τ_A. The $\mu_A(t)$ process contains all the fundamental dynamic elements necessary for describing these dynamic processes. They are the mass (M/N_0), length (b), and friction coefficient (ζ) associated with each statistical Kuhn segment (see eq 4) and the entanglement MW (M_e).

From the data analysis of the $\mu_A(t)$ process, we have obtained the K' value greater than the K value of the $\mu_B(t)$ and $\mu_C(t)$ processes. We attribute this to the larger transverse friction coefficient. The ratio, K'/K, should also be a universal constant for all flexible linear polymers.

From the best N_e value extracted from the analysis of the $\mu_A(t)$ process, we have obtained that there are about 14 monomer (styrene) units per statistical Kuhn segment. This value compares very well with the literature values: 15–20 (Akcasu et al.);[27] 11 (Osaki et al.).[28]

Tube Life: Disentanglement or Constraint Release. So far we have considered the molecular dynamics of a single polymer in a tube, which is not affected by disentanglement (or constraint release) of the neighboring molecules.

In the comparison of the theory with experimental results of nearly monodisperse polymers, this assumption remains valid. However, it would not hold for a broad MWD sample. We have observed that a certain nonlinear blending law due to constraint release is required.[22] Also the diffusion measurements of star molecules (MW = M_s) in the matrix of a linear polymer (MW = M_m)[29] have indicated that the tube life effect becomes very important if the ratio M_s/M_m exceeds a certain value.

For very narrow MWD samples, we have shown that the difference between experimental and theoretical J_e values can be accounted for by considering the MWD, and that the viscosity over the entire MW range (M_e–$70M_e$) can be explained by the present theory without considering the effect of constraint release. This conclusion disagrees with Graessley's explanation for η_0 and J_e.[30,31]

In summary, extensive linear viscoelastic properties of narrow MWD polymers can be successfully explained by the proposed theory. In the data analysis, the theory was used "literally". The consistency observed in the agreements of theory and experiment may allow for exact definition of several fundamental physical quantities in polymer dynamics and viscoelasticity.

Acknowledgment. The author thanks Dr. W. W. Graessley and Professor M. Doi for helpful discussions, Professor D. J. Plazek for providing the information of viscosity and compliance data, and Dr. R. P. White, Jr. for GPC measurement.

Appendix

Consider the primitive chain as a Rouse chain of N_0 segments of length b. And let S_n be the contour length at the nth bead from a certain reference point along the tube. Then the contour length of the primitive chain at a certain time, t, is given as

$$L(t) = S_{N_0}(t) - S_0(t) \tag{A1}$$

The equilibrium value of $L(t)$ is given as

$$L_{eq} = \langle L(t) \rangle = \frac{R^2}{a} = \frac{N_0 b}{(N_e)^{1/2}} \tag{A2}$$

where R is the end-to-end distance of the polymer chain, and a and N_e are the distance and the number of segments between two adjacent entanglements, respectively.

The motion of $S_n(t)$ is described by the following Langevin equation:

$$\zeta \frac{\partial S_n(t)}{\partial t} = \frac{3kT}{b^2} \frac{\partial^2 S_n(t)}{\partial n^2} + f_n(t) \tag{A3}$$

where ζ is the friction coefficient and $f_n(t)$ is a random force:

$$\langle f_n(t) f_m(t') \rangle = 2\zeta kT \delta(t - t') \delta(n - m) \tag{A4}$$

As was discussed by Doi and Edwards, a fictitious tensile force, F_{eq}, as given below, must be assumed at the chain ends.

$$F_{eq} = \frac{3kT}{a} \tag{A5}$$

Hence the boundary condition for eq A3 is

$$\frac{3kT}{b^2} \frac{\partial S_n}{\partial n} = F_{eq} \qquad \text{at } n = 0, N_0 \tag{A6}$$

or

$$\frac{\partial S_n}{\partial n} = l \qquad \text{at } n = 0, N_0 \tag{A7}$$

where

$$l = \frac{b^2}{a} \tag{A8}$$

Equation A3 has the following type of solution which satisfies the boundary condition.

$$S_n(t) = nl + (2/N_0)^{1/2} \sum_p X_p(t) \cos(p\pi n/N_0) \tag{A9}$$

Substituting eq A9 into eq A3, and using the orthonormal properties of the basis function $(2/N_0)^{1/2} \cos(p\pi n/N_0)$, we can obtain

$$\frac{\partial X_p(t)}{\partial t} = -\lambda_p X_p(t) + f_p(t) \tag{A10}$$

where

$$\lambda_p = p^2/\tau_B \tag{A11}$$

with

$$\tau_B = \frac{\zeta b^2 N_0^2}{3kT\pi^2} \tag{A12}$$

and

$$f_p(t) = \frac{1}{\zeta}(2/N_0)^{1/2} \int_0^{N_0} f_n(t) \cos(p\pi n/N_0)\, dn \tag{A13}$$

Substituting eq A9 into eq A1, we obtain

$$\delta L(t) = L(t) - N_0 l = -2(2/N_0)^{1/2} \sum_{p\,\text{odd}} X_p(t) \tag{A14}$$

Since $X_p(t)$'s of different modes do not correlate with each other

$$\langle \delta L(0) \delta L(t) \rangle = \frac{8}{N_0} \sum_{p\,\text{odd}} \langle X_p(0) X_p(t) \rangle \tag{A15}$$

Furthermore, because there is no correlation between $X_p(0)$ and fluctuation $f_p(t)$, we obtain from eq A10

$$\langle X_p(0) X_p(t) \rangle = \langle X_p(0)^2 \rangle e^{-\lambda_p t} \tag{A16}$$

Thus, eq A15 becomes

$$\langle \delta L(0) \delta L(t) \rangle = \frac{8}{N_0} \sum_{p\,\text{odd}} \langle X_p(0)^2 \rangle e^{-\lambda_p t} \tag{A17}$$

Two forces act on the segments along the primitive chain: one is the force of the usual Gaussian spring, $F_s = -(3kT/b^2)(\partial S_n/\partial n)$; the other is the fictitious tensile force $F_{eq} = 3kTl/b^2$. The latter keeps the primitive chain maintaining the contour length L_{eq}. Thus the equilibrium distribution function for S_n is

$$p[S_n] \propto \exp\left[-\frac{3}{2b^2} \int_0^{N_0} \left(\frac{\partial S_n}{\partial n} - \frac{L_{eq}}{N_0} \right)^2 dn \right] \quad \text{(A18)}$$

Using eq A9, eq A18 is rewritten as

$$p[S_n] \propto \exp\left[-\frac{3\pi^2}{2b^2 N_0^2} \sum_p X_p^2 p^2 \right] \quad \text{(A19)}$$

Thus

$$\langle X_p^2 \rangle = \frac{N_0^2 b^2}{3p^2\pi^2} \quad \text{(A20)}$$

and eq A17 becomes

$$\langle \delta L(0) \delta L(t) \rangle = \frac{N_0 b^2}{3} \sum_{p\,\text{odd}} \frac{8}{\pi^2 p^2} \exp(-\lambda_p t) \quad \text{(A21)}$$

Because, a polymer chain moves in a three dimensional space, eq A21 need be corrected for three degrees of freedom as

$$\langle \delta L(0) \delta L(t) \rangle = N_0 b^2 \sum_{p\,\text{odd}} \frac{8}{\pi^2 p^2} \exp(-\lambda_p t) \quad \text{(A22)}$$

Thus $\overline{\delta L(t)}$ defined by eq 10 becomes

$$\overline{\delta L(t)} = (N_0 b^2)^{1/2} \sum_{p\,\text{odd}} \frac{8}{\pi^2 p^2} \exp(-\lambda_p t) \quad \text{(A23)}$$

Using $L = (N_0/N_e^{1/2})b$ (eq A2) and $\delta L = \overline{\delta L(0)} = (N_0)^{1/2} b$ eq 16–18 can be obtained.

References and Notes

(1) Ferry, J. D. "Viscoelastic Properties of Polymers", 3rd ed.; Wiley: New York, 1980.
(2) Bernstein, B.; Kearsley, E. A.; Zapas, L. J. *Trans. Soc. Rheol.* **1963**, *7*, 391.
(3) Wagner, M. H. *Rheol. Acta* **1976**, *15*, 136. **1977**, *16*, 43.
(4) de Gennes, P.-G. *J. Chem. Phys.* **1971**, *55*, 572.
(5) Doi, M.; Edwards, S. F. *J. Chem. Soc., Faraday Trans. 2* **1978**, *74*, 1789.
(6) Doi, M.; Edwards, S. F. **1978**, *74*, 1802.
(7) Doi, M.; Edwards, S. F. **1978**, *74*, 1818.
(8) Doi, M.; Edwards, S. F. **1979**, *75*, 38.
(9) Berry, G. C.; Fox, T. G. *Adv. Polym. Sci.* **1968**, *5*, 261.
(10) Rouse, P. E., Jr. *J. Chem. Phys.* **1953**, *21*, 1271.
(11) Graessley, W. W. *Adv. Polym. Sci.* **1974**, *16*, 1.
(12) Doi, M. *J. Polym. Sci., Polym. Lett. Ed.* **1981**, *19*, 265.
(13) Doi, M. *J. Polym. Sci., Polym. Phys. Ed.* **1983**, *21*, 667.
(14) Mooney, M. *J. Polym. Sci.* **1959**, *34*, 599.
(15) Doi, M. *J. Polym. Sci., Polym. Phys. Ed.* **1980**, *18*, 1005.
(16) Treloar, L. R. G. "The Physics of Rubber Elasticity", 2nd ed.; Oxford University Press: London, 1958.
(17) Mark, J. E. *J. Am. Chem. Soc.* **1970**, *92*, 7252.
(18) Lin, Y.-H. *J. Rheol.* **1984**, *28*, 1.
(19) Saab, H. H.; Bird, R. B.; Curtiss, C. F. *J. Chem. Phys.* **1982**, *77*, 4758.
(20) Curtiss, C. F.; Bird, R. B. *J. Chem. Phys.* **1981**, *74*, 2016.
(21) Curtiss, C. F.; Bird, R. B. **1981**, *74*, 2026.
(22) Lin, Y.-H., unpublished results.
(23) Osaki, K.; Kurata, M. *Macromolecules* **1980**, *13*, 671.
(24) Vrentas, C. M.; Graessley, W. W. *J. Rheol.* **1982**, *26*, 359.
(25) Plazek, D. J.; O'Rourke, V. M. *J. Polym. Sci., Part A-2* **1971**, *9*, 209.
(26) Allen, V. R.; Fox, T. G. *J. Chem. Phys.* **1964**, *41*, 337.
(27) Akcasu, A. Z.; Han, C. C. *Macromolecules* **1979**, *12*, 276.
(28) Osaki, K.; Schrag, J. L. *Polym. J.* **1971**, *2*, 541.
(29) Klein, J.; Fletcher, D.; Fetters, L. J. *Faraday Symp. Chem. Soc.* **1983**, *18*, paper 11.
(30) Graessley, W. W. *Adv. Polym. Sci.* **1982**, *47*, 67.
(31) Graessley, W. W. *Faraday Symp. Chem. Soc.* **1983**, *18*, paper 1.